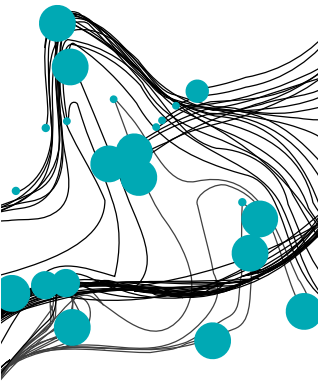

RAM ROBOTICS AND MECHATRONICS

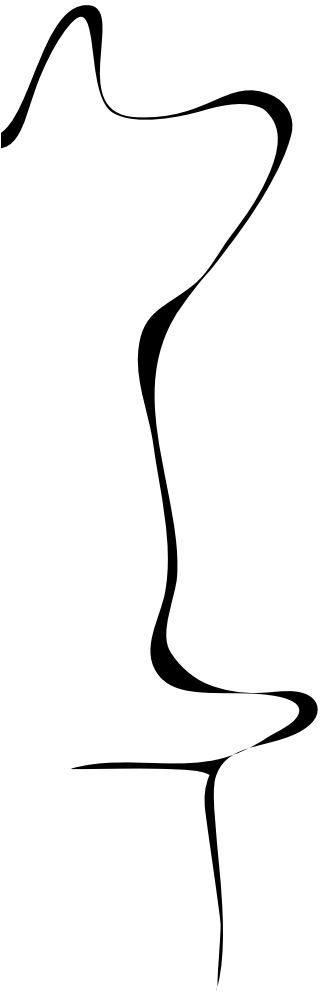

SAFETY METRIC FOR HUMAN-AERIAL ROBOT COLLABORATION, IN PRESENCE OF AERODYNAMIC DISTURBANCES

A. (Adithya) Mylavarapu Naga

MSC ASSIGNMENT

Committee:
prof. dr. ir. A. Franchi
ir. A.N.M.G. Afifi
dr. ir. D. Reidsma

July, 2024

044RaM2024
Robotics and Mechatronics
EEMCS
University of Twente
P.O. Box 217
7500 AE Enschede
The Netherlands

UNIVERSITY OF TWENTE. | TECHMED CENTRE UNIVERSITY OF TWENTE. | DIGITAL SOCIETY INSTITUTE

Summary

When considering close interaction between a human & an aerial robot, one aspect that is unique to this scenario with respect to other ground-based robotic platforms is the presence of wind disturbances that act on the aerial robot. In order to realize that aerial robots can coexist & collaborate with humans, we must be able to guarantee the safety of humans even in the presence of wind disturbances.

To ensure the safety of human collaborators in such scenarios, this thesis aims to establish a comprehensive safety metric that guides the robot's motion during such interactions. The aerial robot considered for defining a safety metric is a hexarotor with a tilted-propeller configuration (tilt-hex). In the presence of a known wind disturbance, an aerodynamic model estimates the addition wrench this disturbance provides. The deviation due to this disturbance is then used to construct a safety metric that ensures the aerial-robot's motion is guided and it operates safely within the environment.

In the presence of wind, this safety metric ensures that the aerial robot maintains a safe distance with the human collaborator. The controller that embeds this safety metric is a Non-Linear Model Predictive Controller (NMPC). The controller generates a control inputs, such that the safety constraint is satisfied throughout the trajectory. Thereby ensuring safe operation with the human collaborator.

Simulations were performed to obtain and construct this safety metric and the system was tested with various wind conditions. The system's performance under these conditions was then evaluated to determine if the safety metric remained satisfied throughout the whole trajectory.

Finally, a brief conclusion and potential directions for future work have been detailed.

Acknowledgements

First and foremost, I would like to express my sincere gratitude to my supervisor, Amr Afifi, for his support and invaluable guidance throughout my thesis journey. His expertise in the field of control, robotics, and research helped me grasp concepts quickly. I am particularly grateful for his insightful feedback, constant encouragement, and the numerous opportunities he provided for me to expand my knowledge and skills.

I would also like to extend my appreciation to Antonio Franchi, the chair of my thesis project. His enthusiasm for the group and the fields of Multi-rotor aerial vehicles and Control was inspiring. His ideas on clarity helped me with the way i approach problems. I am deeply grateful for the opportunity to work on such cutting-edge research under his supervision,

Finally, I want to acknowledge the incredible support I received from my family and friends during this challenging but rewarding endeavor. Their encouragement and belief in me have been a constant source of motivation.

Adithya Mylavarapu Naga
Saturday 20th July, 2024

Contents

List of Figures

1 Introduction

The field of unmanned aerial vehicles (UAVs) has seen significant advancements, particularly with the development of multirotor systems such as hexarotors. In recent years, UAVs have integrated themselves into various domains, including search and rescue [10, 7] environmental monitoring [9, 14], cooperative tasks, and physical interaction tasks [16, 21, 15, 5]. As technology advances, UAVs are increasingly operated in close proximity to humans , especially in the case of human-aerial robot collaboration. Therefore, it is necessary to consider robust metric to ensure the safety of human operators. These metric must also include aerodynamic disturbances, to be more precise the effect of wind disturbance. In this case, the wind disturbances directly affects UAV's stability and trajectory, hence the task at hand.

1.1 Problem Statement

During such interactions between the human operator and the UAV, ensuring a safe operation is important and challenging in the presence of wind disturbances. Wind can cause significant deviations in a UAV's expected pose, leading to potential safety hazards. Therefore, it is essential to develop safety metric that guides UAV motion and ensure safe operation even under windy conditions.

1.2 Traditional Approaches

Traditionally, quadrotors have been the main platform used in both research and industry. These systems are underactuated, meaning they cannot control all six degrees of freedom (DOFs) independently. For a three-dimensional task, a UAV system must maneuver in six DOFs: translational motion along the X, Y, and Z axes, and rotational motion around the X, Y, and Z axes (roll, pitch, yaw). A quadrotor provides only four primary control variables: total thrust in the z-direction, roll, pitch, and yaw. Translational motion along the X and Y axes is achieved indirectly by tilting the quadrotor [11].

This underactuation limits the UAV's ability to perform complex maneuvers and maintain stability in dynamic environments, such as those with wind disturbances. It is crucial to have the ability to control all six DOFs independently, which is achievable with fully-actuated systems. Figure.1.1a,1.1b shows the multirotor platforms that are actively being researched at University of Twente and LAAS-CNRS, France.

(a) Underactuated Quadrotor

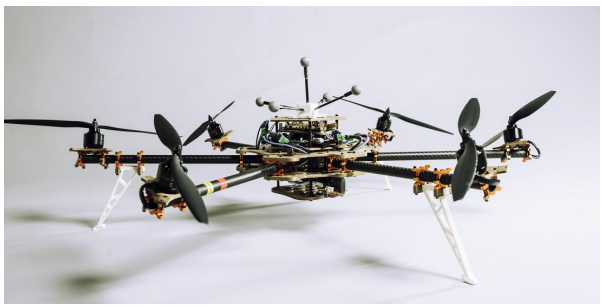

(b) Fully-actuated Hexarotor (FiberTHex)

Figure 1.1: Multirotor platforms of UT & LAAS-CNRS

1.3 Brief Description of the System

The system used in this thesis is a fully-actuated tilted-axis hexarotor. A tilted-axis hexarotor is a type of UAV equipped with six rotors, providing enhanced stability, maneuverability, and payload capacity compared to traditional quadrotors. The primary objective of this research is to develop a comprehensive safety metric that guide the hexarotor's motion during close interactions with humans, ensuring safety even in the presence of wind disturbances.

An aerodynamic model is used to estimate the additional force and torque provided by known wind disturbances. The deviation from the expected pose due to these disturbances is then used to construct a safety metric. This metric ensures that the UAV maintains a safe distance from human collaborators.

The thesis hypothesis is to incorporate a Non-Linear Model Predictive Controller (NMPC) with the developed safety metric, it is possible to generate control inputs that satisfy safety constraints throughout the UAV's trajectory, thereby ensuring safe operation in the presence of wind disturbances.

1.4 Methodology and Contributions

The plan of approach of this thesis includes,

1. Developing an aerodynamic model to estimate the wind disturbance and an expected deviation.
2. Constructing a safety metric for fully-actuated tilted-axis hexarotor that considers the aerodynamic model.
3. The control strategy includes implementation of an NMPC that incorporates the safety metric for optimal control within the environment.
4. Validation of the proposed safety metric and control strategy through simulations under various wind conditions. With the aim to evaluate the metric performance throughout the UAV's trajectory.

The system's safety metric is simulated under various wind conditions and the performance is evaluated with the aim to guide the UAV's motion in environments.

1.5 Organization of the Report

The structure of this thesis report is organized as follows:

1. **Chapter 2: Background Literature** - Discusses related work and highlights gaps in existing safety measures for UAVs.
2. **Chapter 3: Design & Modeling** - Details the aerodynamic modeling, safety metric construction, and control strategy implementation.
3. **Chapter 4: Safety Metric** - Details the construction of the metric.
4. **Chapter 5: Non-Linear Model Predictive Controller** - Details how the controller is formulated.
5. **Chapter 6: Simulation & Results** - Presents the results of simulations conducted under various wind conditions, evaluating the system's performance.
6. **Chapter 7: Discussion and Conclusion** - Summarizes the findings, discusses the implications of the research, and suggests potential directions for future work.

2 Background Literature

The use of UAVs for various applications have grown rapidly over the past decade. In fields such as, search and rescue, environmental monitoring and delivery services. The increase in research makes UAV systems robust and accurate. This enables such systems to operate with close proximity to humans, making it necessary to have robust safety measures during such interactions. Particularly in collaboration tasks, it is important to have a safety metric that guides the robot motion in presence of external disturbances.

An important factor that affects the performance of a UAV during human-aerial collaboration is aerodynamic disturbances, to be precise, wind. Wind disturbances can affect the UAV's trajectory, particularly high winds speeds impacts the trajectory even in the presence of a well defined controller.

The background literature aims to have a understanding of existing UAV research such as the design and control of tilted propeller hexarotor systems. Existing UAV safety methods and Aerodynamic modeling that accounts for wind disturbance and a control strategy to guide the robot's motion in the presence of such a disturbance. More important, a safety metric that helps the system avoid collision with the human operator in a windy environment.

Design and Control of Tilted Propeller Hexarotor systems: [18] designs a fully-actuated hexarotor system with tilted propellers. Tilting the propeller will enable a horizontal thrust component thereby offering enhanced maneuverability. This design has more control degrees of freedom making it fully-actuated. The control method here is feedback linearization. [2] deals with an extended system including a robotic arm, making it an aerial manipulator. With the objective of physical interaction with a human operator. The control framework used here is an admittance control paradigm. When considering only a safety distance it is beneficial to consider an optimal control problem (OCP) and use a Non-Linear Model predictive control, a method known for its ability to handle complex systems with constraints. NMPC is chosen for its capability to predict the system's future behavior and optimize control inputs accordingly.

Safety Methods and Control Strategy : [6] uses this control method to handover an object to a human operator. An NMPC framework is used to handle multiple tasks using constraints [3] presents an algorithm that uses an NMPC to decide the control authority. It evaluates whether safety and/or task-related rules are being adhered to, this relates to the degree of authority shared between the operator and the controller. [19] details an Obstacle avoidance using an NMPC. The algorithm was implemented on a mobile robot. In NMPC, a cost function is formulated to minimize the error between a reference state and the current state. Here, the obstacle avoidance is included as a constraint in the optimization problem.

Safety Distance under Wind Disturbance :[12] considers the safety of a UAV in the application of electrical line inspection. Aimed to plan a safe flight path in the presence of an unknown wind. They use a floating threshold to maintain a safe distance to the line that is based on sensor weights and a "wind scale". **Wind Prediction :**[1] uses a complex computational fluid dynamics (CFD) approach to predict wind using deep learning. These are valid approaches to estimate the local wind speed. The safety metric will depend on the distance representation (maximum deviation of the states) for a wind force.

Aerodynamic Modeling and Propeller Coefficients : The works of Teodor Tomić on metric wind estimation [23] gives a brief overview of the relation between true airspeed and freestream velocity. [17] gives a detailed look at propeller aerodynamics and a control wrench of a propeller. The drag effect on the rotational and translational dynamics are

detailed. With this method, one can estimate the force and torque of the corresponding wind. [24] details that the presence of wind disturbance affects the propeller properties, thereby changing the coefficients of force and torque. Therefore, it is vital to look at the change of coefficients for the particular propeller. These are obtained experimentally. [4, 13, 8] look at the different sized propeller characteristics for various advance ratios. [20] performs a similar analysis of the coefficient of thrust, power for various advance ratios. The relation between advance ratio and the wind speed will be detailed in the following chapter.

The existing literature provides a brief about human-aerial collaboration system. Research in tilted-axis hexarotor design and control explores maneuverability and full actuation, offering greater control over the UAV's motion. Existing safety methods, primarily focused on NMPC-based control strategies, handle complex tasks with constraints, such as object handover and obstacle avoidance. These methods are robust and the idea is to incorporate a safety distance for wind as an constraint to respect during the human-aerial collboartion task.

Background into aerodynamic modeling and propeller coefficients details the effects of wind on UAV performance. This is crucial for developing accurate wind models and control strategies. Existing safety distance metric under wind disturbances incorporate a safe distance to the task-based models. A more dynamic and adaptive safety metric, incorporating wind change to ensure safe human-aerial collaboration under various wind conditions. The existing literature is further explored in this thesis to develop a system that can incorporate wind disturbance during a human-aerial collaboration task.

With the obtained background, the following chapters will delve into specific aspects of this background. The next chapter will focus on modeling the tilted-axis hexarotor, incorporating propeller aerodynamics into the dynamics. This includes modeling wind as a component of drag and considering propeller properties. Following that, the chapter on safety metric will detail the construction of a safety metric under various wind conditions, for safe human-aerial interaction. Finally, the thesis will present simulations conducted on this system for a particular case, demonstrating the practical application of the developed models and safety measures.

3 Modeling

This chapter presents a comprehensive model for a fully-actuated hexarotor with tilted propellers, focusing on both rotational and translational dynamics. Proper definition of the model is crucial for accurate control and stability, especially in the presence of external factors such as wind. This dynamic model also incorporates the effect of aerodynamic disturbances. Compared to a traditional dynamics equation of a hexarotor as defined in [18]. Extending on this background, this model incorporates additional rotor aerodynamics taking into considerations the drag forces on both the translational and rotational dynamics.

Table 3.1: Overview of the main symbols used in this section.

Definition	**Symbol**
World Frame	$\mathcal{F}_W$
Body Frame	$\mathcal{F}_B$
Position of frame $\mathcal{F}_W$ origin	O_B
Position of frame $\mathcal{F}_B$ origin	O_{Pi}
Position of $\boldsymbol{O_B}$ in $\mathcal{F}_W$	$\boldsymbol{p}$
Position of $\boldsymbol{O}_{Pi}$ in $\mathcal{F}_B$	${}^B\boldsymbol{p}_i$
Inertia matrix	$\mathbf{I_B}$
Aerodynamic disturbances torque	$\boldsymbol{\tau_{aero}}$
Input torque	$\boldsymbol{\tau}$
Thrust torque	$\boldsymbol{\tau_{thrust}}$
Drag torque	$\boldsymbol{\tau_{drag}}$
Rotation matrix from $\mathcal{F}_{Pi}$ to $\mathcal{F}_B$	${}^B\boldsymbol{R}_{Pi}$
Thrust force of the i-th propeller	$\mathbf{T_{thrust_i}}$
Drag force of the i-th propeller	$\mathbf{T_{drag_i}}$
Total force matrix	$\mathbf{F}(\alpha, \beta, \lambda_\mathbf{x})$
Wind velocity	$\mathbf{V_W}$
Linear velocity of the i-th propeller	$\mathbf{V_{Pi}}$
Drag coefficient matrix	$\mathbf{A_{drag}}$
Total thrust magnitude	$\mathbf{T_{thrust}}$
Freestream velocity in propeller frame	$\mathbf{v}_\infty$
Advance ratio	$\mathbf{J}$
Force coefficient	$\mathbf{k_f}$
Torque coefficient	$\mathbf{k_t}$

3.1 Modelling for a Fully-Actuated TiltHex with Tilted Propellers

The following are the notation for the static system description, The inertial frame is defined as $\mathcal{F}_W$ whose axes are $\{\mathbf{X_W}, \mathbf{Y_W}, \mathbf{Z_W}\}$ and the hexarotor body frame is defined as $\mathcal{F}_B$ with $\{\mathbf{X_B}, \mathbf{Y_B}, \mathbf{Z_B}\}$. The propeller frame at center of mass (COM) of the propeller is defined as $\mathcal{F}_{P_i}$ where $i = 1 \dots 6$, with origin $\mathbf{O_{P_i}}$ and axes $\{\mathbf{X_{P_i}}, \mathbf{Y_{P_i}}, \mathbf{Z_{P_i}}\}$. The position $\boldsymbol{p} \in \mathbb{R}^3$ of $\boldsymbol{O_B}$ in $\mathcal{F}_W$ and ${}^B\boldsymbol{p}_i \in \mathbb{R}^3$ is the position of $\boldsymbol{O}_{Pi}$ in $\mathcal{F}_B$.

Let the rotation matrix ${}^W\mathbf{R}_B \in \mathrm{SO}(3)$ represent the orientation of $\mathcal{F}_B$ with respect to $\mathcal{F}_W$ and ${}^B\mathbf{R}_{P_i} \in \mathrm{SO}(3)$ represent the orientation of $\mathcal{F}_{P_i}$ with respect to $\mathcal{F}_B$, for $i = 1 \dots 6$. The orientation of frame $\mathcal{F}_{P_i}$ w.r.t $\mathcal{F}_B$ is given by combination of rotations between ${}^B\mathbf{R}_{P_i} = \mathbf{R}_z(\lambda_i)\mathbf{R}_x(\alpha_i)\mathbf{R}_y(\beta_i)$. Here, λ_i decides the space between each propeller, defined as $\lambda_i = (i-1)\frac{\pi}{3}$. The tilting of the i-th propeller is represented by α_i and β_i. The complete

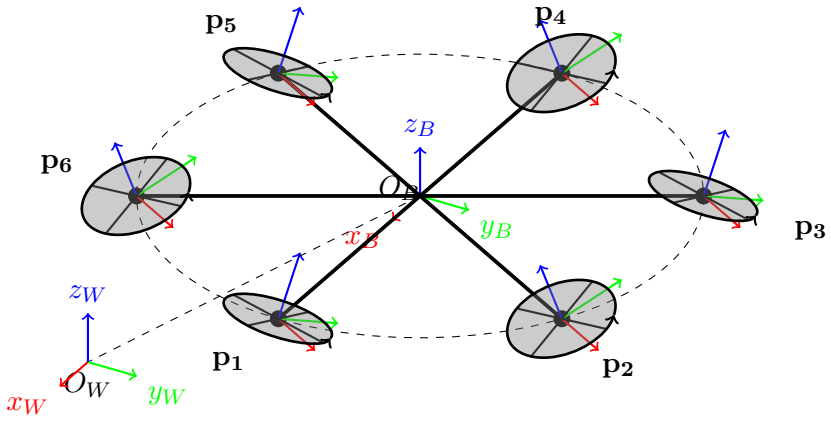

Figure 3.1: Minimal Representation of the TiltHex

dynamics of the hexa-rotor is derived using the Newton-Euler approach. A brief about the rotational and translational dynamics are as follows.

3.1.1 Rotational Dynamics

The rotational dynamics are

$$\mathbf{I_B}\dot{\omega}_\mathbf{B} = -\omega_\mathbf{B} \times \mathbf{I_B}\omega_\mathbf{B} + \tau + \tau_\mathbf{aero} \tag{3.1}$$

Above, $\mathbf{I_B}$ is the inertia matrix, $\omega_\mathbf{B} \in \mathbb{R}^3$ is the angular velocity in the body frame, $\boldsymbol{\tau_{aero}}$ accounts for aerodynamic disturbances, and $\boldsymbol{\tau}$ is the torque provided to the system, which is

$$\tau = \tau_\mathbf{thrust} + \tau_\mathbf{drag} \tag{3.2}$$

Where, $\boldsymbol{\tau_{thrust}}$ and $\boldsymbol{\tau_{drag}}$ are the 6 propeller's thrusts and drags.

$$\tau_\mathbf{thrust} = \sum_{\mathbf{i=1}}^{\mathbf{6}} ({}^\mathbf{B}\boldsymbol{p}_\mathbf{i} \times {}^\mathbf{B}\boldsymbol{R}_\mathbf{Pi}\mathbf{T}_{\mathbf{thrust_i}}) \tag{3.3}$$

$$\tau_\mathbf{drag} = \sum_{\mathbf{i=1}}^{\mathbf{6}} ({}^\mathbf{B}\boldsymbol{R}_\mathbf{Pi}\mathbf{T}_{\mathbf{drag_i}}) \tag{3.4}$$

We can write τ as the following,

$$\tau = \mathbf{H}(\alpha, \beta, \lambda, \mathbf{L_X})\mathbf{u} \tag{3.5}$$

3.1.2 Translational Dynamics

The translational dynamics are,

$$m\ddot{\boldsymbol{p}} = m \begin{bmatrix} 0 \\ 0 \\ -g \end{bmatrix} + {}^\mathbf{W}\mathbf{R_B}\mathbf{F}(\alpha, \beta, \lambda)\mathbf{u} + \mathbf{f_{aero}} \tag{3.6}$$

Where, $\mathbf{F}(\alpha, \beta, \lambda) \in \mathbb{R}^{3\times6}$, is the matrix that represents the total force produced by the propellers.

$$\mathbf{F}(\alpha, \beta, \lambda)\mathbf{u} = \sum_{\mathbf{i=1}}^{\mathbf{6}} ({}^\mathbf{B}\boldsymbol{R}_\mathbf{Pi}\mathbf{T}_{\mathbf{thrust_i}}) \tag{3.7}$$

The terms $\mathbf{T}_{\mathbf{thrust_i}}$ and $\mathbf{T}_{\mathbf{drag_i}}$ are elaborated in the rotor aerodynamics section.

3.2 Rotor Aerodynamics (f_{aero} & τ_{aero})

To incorporate the effect of wind in the model, [17] considers the blade flapping and drag. They are elaborated as follows, blade flapping and induced drag are key factors in the natural stability of hexarotor. These forces act on the rotor plane, impacting the translational and rotational dynamics of the hexarotor.

Aerodynamic drag, caused by blade flapping, becomes particularly relevant during forward flight. The advancing rotor blade experiences higher tip velocity and generates more lift than the retreating blade. Due to the flexibility of rotor blades, this imbalance causes them to flap.

The i-th propeller creates a force vector applied at O_{Pi} and directed along Z_{Pi} expressed in the propeller frame $\mathcal{F}_{Pi}$

$$\mathbf{T_{thrust,i}} = \begin{bmatrix} 0 & 0 & k_f \varpi_i^2 \end{bmatrix} \tag{3.8}$$

The drag moment generated by the i-th propeller acts in the opposite direction of the propeller angular velocity and is expressed in $\mathcal{F}_{Pi}$

$$\mathbf{T_{drag,i}} = \begin{bmatrix} 0 & 0 & (-1)^i k_t \varpi_i^2 \end{bmatrix} \tag{3.9}$$

The linear velocity that the i-th propeller experiences is given by

$$\mathbf{V_{Pi}} = {}^{\mathbf{B}}\mathbf{R_W}(\dot{\mathbf{p}} - \mathbf{V_W}) + \omega_{\mathbf{B}} \times {}^{\mathbf{B}}\mathbf{P_i} \tag{3.10}$$

The effect of drag force on the translational dynamics is given as,

$$\mathbf{f_{aero}} = -\mathbf{T_{thrust}}.\mathbf{A_{drag}}.{}^{\mathbf{B}}\mathbf{R_W}(\dot{\mathbf{p}} - \mathbf{V_W}) \tag{3.11}$$

Here, $\mathbf{A_{drag}}$ is the is the drag coefficient matrix. and $\mathbf{T_{thrust}}$ is the total thrust magnitude

$$\mathbf{A_{drag}} = \begin{bmatrix} c_a + c_{dx} & -c_b & 0 \\ c_b & c_a + c_{dy} & 0 \\ 0 & 0 & 1 \end{bmatrix} \tag{3.12}$$

$$\mathbf{T_{thrust}} = \mathbf{K_f} \sum_{\mathbf{i}} \varpi_{\mathbf{i}}^{\mathbf{2}} \tag{3.13}$$

The effect of the drag forces on the rotational dynamics is given as,

$$\tau_{\mathbf{aero}} = -\sum_{\mathbf{i}} ({}^{\mathbf{B}}\mathbf{P_i} \times \mathbf{T_{thrust,i}}) \times (\mathbf{A_{drag}}\mathbf{V_{pi}}) \tag{3.14}$$

The hexarotor **dynamical model** in the presence of wind can therefore be written as,

$$m\ddot{\boldsymbol{p}} = m \begin{bmatrix} 0 \\ 0 \\ -g \end{bmatrix} + \frac{1}{m} {}^{\mathbf{W}}\mathbf{R_B}\mathbf{F}(\alpha, \beta, \lambda)\mathbf{u} + \mathbf{f_{aero}} \tag{3.15}$$

$$\dot{\omega}_{\mathbf{B}} = -\mathbf{I_B^{-1}}(\omega_{\mathbf{B}} \times \mathbf{I_B}\omega_{\mathbf{B}}) + \mathbf{I_B^{-1}}\mathbf{H}(\alpha, \beta, \lambda, \mathbf{L_x})\mathbf{u} + \tau_{\mathbf{aero}} \tag{3.16}$$

Where Equations.3.15 and 3.16 are the translational and rotational dynamics with the additional aerodynamic drag term. The terms $\mathbf{F}(\alpha, \beta, \gamma)\mathbf{u}$ and $\mathbf{H}(\alpha, \beta, \gamma, \mathbf{L})\mathbf{u}$ are expanded in the Appendix.A.

3.2.1 Wind and Freestream Velocity on Propeller Force and Torque Coefficients

When a propeller experiences external disturbances such as wind, the freestream velocity impacting the propeller changes. It can be understood as the relative airspeed that a propeller encounters as it moves through air. In the presence of wind, this changes. Therefore, it is important to understand propeller's aerodynamics under the influence of wind disturbance.

The air surrounding the propellers is disturbed in the presence of wind. This affects the propeller's dynamics, the advance ratio of the propeller is one such parameter that changes. It is related to the freestream velocity ($\mathbf{V}_\infty$) and the propeller's velocity (ω). It is mathematically defined as $\mathbf{J} = \frac{\mathbf{V_z}}{\omega \mathbf{D}}$, where D is the propeller's diameter. This change in the advance ratio is also related to the propeller speed. The coefficients of force and torque are dependent on the advance ratio and propeller speed as they determine how these coefficients change with a change in the advance ratio. This can be formally defined as $\mathbf{k_f} = \mathbf{f}(\varpi, \mathbf{J})$ and $\mathbf{k_t} = \mathbf{f}(\varpi, \mathbf{J})$. [22], describes this connection between freestream velocity, advance ratio, and the coefficients of force and torque . The freestream velocity of the i-th propeller in the propeller frame is given by the following equation.

$$\mathbf{v}_\infty = {}^{\mathbf{P_i}}\mathbf{R_B} \cdot ({}^{\mathbf{B}}\mathbf{R_W}(\dot{\mathbf{p}} - \mathbf{V_W}) + \omega_\mathbf{B} \times {}^{\mathbf{B}}\mathbf{P_i}) \tag{3.17}$$

The vertical component of the freestream velocity, $\mathbf{V_Z}$, is represented as:

$$\mathbf{V_Z} = \begin{bmatrix} 0 & 0 & \mathbf{V}_\infty \end{bmatrix}^\mathbf{T}$$

This relationship between the advance ratio, propeller speeds, and freestream velocity can be determined experimentally. In [20], an experimental analysis on various propellers is conducted, detailing the changes in force and torque coefficients at different propeller speeds ϖ and advance ratios $\mathbf{J}$. From the definition of advance ratio, the size of the propeller impacts this relation. For a propeller of the size **13**" × **8**" the relationship between the coefficient of force and torque is illustrated in Figure.3.2

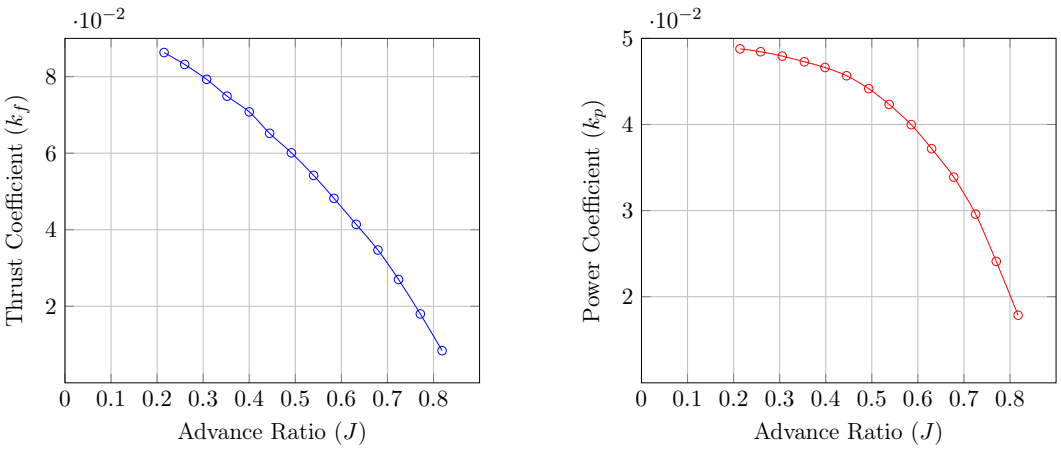

Figure 3.2: Change in the coefficients of force and power for various advance ratios (Propeller Size : 13" x 8")

The torque generated by the propeller in relation to the power is defined as $\mathbf{k_t} = \frac{\mathbf{k_P}}{\mathbf{2}\pi\omega}$. The relation $\mathbf{k_f} = \mathbf{f}(\varpi, \mathbf{J})$ and $\mathbf{k_t} = \mathbf{f}(\varpi, \mathbf{J})$, is then realized using a $\mathbf{2^{nd}}$ order model. This is used to update the coefficients during simulations.

This chapter developed a dynamic model for a fully-actuated hexarotor with tilted propellers, focusing on the crucial inclusion of aerodynamic disturbances and drag forces. The model

builds on traditional hexarotor dynamics by incorporating drag forces in both translational and rotational dynamics. Changes in freestream velocity and advance ratio due to wind influence the force and torque coefficients of the propellers. These relationships, determined experimentally, are crucial for adjusting the model to maintain accuracy.

The additional $\mathbf{f_{aero}}$ and $\tau_{\mathbf{aero}}$ produce a deviation in the UAV's trajectory (expected states). This deviation is studied in the following chapter. And it is crucial for constructing a safety metric.

4 Safety Metric

When a hexarotor is operating around a human in a windy evironment, there is expected to be a deviation in position of the drone due to the wind. This can potentially lead to a crash. Hence, there is a need to understand this deviation and construct a metric that can ensure that the hexarotor can maintain a safe distance from the human operator. The safety metric includes a set of position deviations from the expected trajectory due to the wind disturbance. These deviations can be incorporated into a model, which predicts the extent of deviation for a given wind velocity. In the Chapter3, an expression for the dynamics model of the hexarotor was derived. As detailed in Equation.3.10, the linear velocity experienced by the i-th rotor contains the additional $\mathbf{V_W}$ wind velocity term. Assuming that the wind speed is not negligible, we can estimate a position deviation of the system by including this disturbance ($\mathbf{V_W}$) to the system dynamics.

For a known wind velocity, assuming that the controller dynamics does not include aerodynamic modeling. There is bound to be deviation from the expected states of the system because of the additional wind disturbance. With this, the effect of wind on the overall position deviation of the hexarotor can be represented. The safety metric should include a proper estimate of this position deviation. Therefore, for particular wind magnitude, there is a need to analyze the wind direction that results in the maximum deviation of the position. Let us call this wind direction as critical wind direction. The following section will detail how to this is obtained.

4.1 Constructing the Safety Metric

The average wind speed in the Netherlands is around $\mathbf{5}\,\mathrm{m/s}$[1], with high speed around $\mathbf{10}\,\mathrm{m/s}$ for a normal day. It is important to consider the deviation of tilt-hex position for the wind speeds spanning between $\mathbf{1}\,\mathrm{m/s}$ and $\mathbf{10}\,\mathrm{m/s}$ in the order of $\mathbf{1}, \mathbf{2}, \ldots \mathbf{10}\,\mathrm{m/s}$. Therefore, **10** simulations were conducted, one for each of these **10** wind magnitudes.

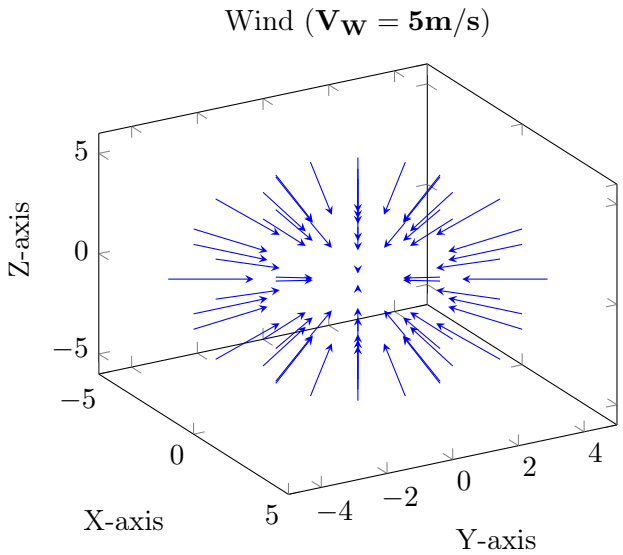

Figure 4.1: Wind vectors used to evaluate Critical Wind

Fig.4.1 illustrates the various wind vectors considered for estimating the critical wind direction for a magnitude of $\mathbf{5m/s}$. To obtain a robust safety metric, it is important to

[1] Annual Wind Speed in the Netherlands, Current Results, accessed July 18, 2024

understand the impact of directionality in aerodynamics. Therefore, It is necessary to consider wind from all possible directions. For one simulation (i.e., for a particular wind magnitude), A total of **62** different wind directions are considered. Distributing the vectors evenly over a sphere ensures that all directions are adequately covered. Since directionality impacts the results in aerodynamic testing, with a step size of $\mathbf{30}^\circ$ deg, the vectors cover the sphere sufficiently without significant gaps, providing a good approximation of all possible directions of wind.

For a particular wind magnitude, the biggest position deviation out of the simulation is then considered to be critical i.e., For this particular wind direction, deviation from the expected position was observed to be the largest in a single simulation.

4.2 Obtaining the Safety Metric

In order to make the safety metric robust to any trajectory, we must consider the case of hover, a linear trajectory in x, y, and z axis individually and analyze the deviation of position. Obtaining a Safety Metric for each case involved performing simulations for all the various wind velocities.

$\mathbf{V_w(m/s)}$	**Maximum Position Deviation Error**				**Std. Dev. (m)**
	Hover (m)	**Trajectory in**			
		X(m)	**Y(m)**	**Z(m)**	
1.0000	0.0056	0.0057	0.0057	0.0057	0.00004
2.0000	0.0113	0.0113	0.0113	0.0138	0.00108
3.0000	0.0169	0.0566	0.0298	0.0504	0.01590
4.0000	0.0799	0.0916	0.0997	0.0962	0.00747
5.0000	0.1172	0.1477	0.1406	0.1388	0.01139
6.0000	0.1755	0.1943	0.1933	0.1893	0.00751
7.0000	0.2215	0.2385	0.2365	0.2319	0.00657
8.0000	0.2628	0.2782	0.2783	0.2724	0.00631
9.0000	0.3015	0.3165	0.3196	0.3160	0.00701
10.0000	0.3385	0.3534	0.3597	0.3565	0.00812

Table 4.1: Safety Metric : Maximum Position Deviation

Following is a brief about the simulation. The system was simulated under the disturbance of wind for 5 seconds with the aim to observe the maximum deviation in position. This disturbance included wind vectors starting from $\mathbf{1m/s}, \mathbf{2m/s} \ldots$ upto $\mathbf{10m/s}$. For the first case, the hexarotor was tasked to maintain a hover condition under the various disturbances. For the cases 2,3 & 4, the hexarotor was tasked to follow a trajectory of **1m** along the X axis, Y and Z direction respectively. The deviations because of the wind disturbance $\mathbf{v_w}$ are tabulated in Table.4.1. These are then used to fit a 4th order model that can estimate a deviation in position for a given wind velocity. This safety distance is added as a constraint to the NMPC problem. This will be detailed in the next chapter.

The standard deviation of the position error for trajectory in various directions is $\mathbf{0.00714m}$. This indicates, the direction of trajectory doesn't influence the position deviation error. Since, the hexarotor is fully actuated, this can be extended to more complicated trajectories because of the consideration of sphere detailed earlier, this leads to a good approximation of the deviation for all directions. This is explored later in the Discussion 7.1

5 Non-Linear Model Predictive Controller

In the context of a trajectory tracking task, the aim of a Non-Linear Model Predictive Controller (NMPC) is to track the position states of the system $\mathbf{x(t)}, \mathbf{y(t)}, \mathbf{z(t)}$ to a desired trajectory closely. This is achieved by solving an Optimal Control Problem (OCP) at each time step to determine the control inputs $\mathbf{u(t)}$ that minimize the deviation from the desired trajectory. The NMPC is a model based approach that also takes into account the dynamic model of the system. It achieves this minimization to a desired trajectory while also considering the system constraints and parameters. An NMPC is robust because of its ability to look in the future, this is the prediction horizon. This horizon defines the number of time steps over which the controller solves the OCP and optimizes the system's performance adding to it's robustness. Following is formal definition of the structure of NMPC.

The NMPC problem tries to achieve a optimal solution for a trajectory tracking problem. For this we consider the state space model for controlling the system.

$$\mathbf{x} := \begin{bmatrix} \mathbf{p}^T & \mathbf{R_B}^T & \dot{\mathbf{p}}^T & \omega_{\mathbf{B}}{}^T \end{bmatrix}^T \tag{5.1}$$

$$\mathbf{u} := [\mathbf{u_1} \dots \mathbf{u_n}]^T \tag{5.2}$$

The general dynamic equation of the system can be described as,

$$\dot{\mathbf{x}} = \mathbf{f}(\mathbf{x(t)}, \mathbf{u(t)}) \tag{5.3}$$

Here, $\mathbf{x} \in \mathbb{R}^{n_x}$ is the state vector and $\mathbf{u} \in \mathbb{R}^{n_u}$ is the input vector, with $\mathbf{n_x} = 12$ and $\mathbf{n_u} = 6$. Consider the reference state trajectory to be tracked as $\mathbf{y^r(t)}$, where $\mathbf{r}$ refer to the refernce, this is expanded as,

$$\mathbf{y^r(t)} := \begin{bmatrix} \mathbf{p}^r(t) & \mathbf{R_B}^r(t) & \dot{\mathbf{p}}^r(t) & \omega_{\mathbf{B}}{}^r(t) \end{bmatrix}^T \tag{5.4}$$

5.1 Objective Function

The NMPC is tasked to track this reference trajectory by solving the following OCP. The system model is discretized using $\mathbf{4^{th}}$ order Runge-Kutta method. This results in a discrete model similar to Eq.5.3. It is included in the objective function. The Objective function is formally defined as follows ...

$$\begin{aligned} \min_{\substack{x_0,\dots,x_{N-1} \\ u_0,\dots,u_{N-1}}} \quad & \sum_{k=0}^{N-1} \|\mathbf{y}(k) - \mathbf{y}^r(k)\|^2_{\mathbf{W}} + \|\mathbf{y_e}(k) - \mathbf{y_e}{}^r(k)\|^2_{\mathbf{W}_e} \\ \text{Subject to} \quad & \mathbf{x}(0) = \mathbf{x}_0, \\ & \mathbf{x}(k+1) = f(\mathbf{x}(k), \mathbf{u}(k)); \quad k \in \{0, 1, ..., N-1\}, \\ & \|\mathbf{x}(k) - \mathbf{x}_{\text{obs}}(k)\| \geq (r_{\text{rob}} + r_{\text{obs}}) + d_{\text{safe}} \\ & \mathbf{u}_{\min} \leq \mathbf{u}(k) \leq \mathbf{u}_{\max} \quad k \in \{0, 1, ..., N-1\} \end{aligned} \tag{5.5}$$

The term $\|\mathbf{y}(k) - \mathbf{y}^r(k)\|^2_{\mathbf{W}}$ is the running cost computes the deviation of the state $\mathbf{y}(k)$ form the reference states $\mathbf{y^r}(k)$. Here, k is the controller step, the term $\mathbf{W} \in \mathbb{R}^{n_x \times n_x}$ is the weight matrix. The optimization problem generates inputs for the prediction horizon $(u_0 \dots u_{N-1})$

that minimize this state deviation to the reference states. The term $\|\mathbf{y_e}(k) - \mathbf{y_e}^r(k)\|^2_{\mathbf{W}_e}$ is the terminal cost with the subscript $\mathbf{e}$, it is evaluated by applying the weight $\mathbf{W_e} \in \mathbb{R}^{n_x \times n_x}$ to the last state prediction and reference $\mathbf{y_e}(k), \mathbf{y_e}(k)^r$ at $k = N$. the control input constraint $\mathbf{u}_{\min} \leq \mathbf{u}(k) \leq \mathbf{u}_{\max}$ ensure that the inputs are in a desired range. There is an additional obstacle avoidance constraint $\|\mathbf{x}(k) - \mathbf{x}_{\text{obs}}(k)\| \geq (r_{\text{rob}} + r_{\text{obs}}) + d_{\text{safe}}$ ensures that the system maintains a safe distance from the obstacles r_{rob} & r_{obs} are the radius of the hexarotor and human respectively. d_{safe} is the additional safety from the safety metric, detailed here 5.2.

The objective function ensures that the states of the system reach desired reference state trajectory with the weighted running and terminal cost. The prediction horizon of the NMPC ensures that the control inputs ensure the system follow the trajectory whilst also respecting the constraints.

5.2 Incorporating the Safety Metric in the Controller

The influence of the wind on the deviation of the states was detailed in the previous section 4. It is important to incorporate this additional deviation in the constraint of NMPC to ensure that the additional wind disturbance does not cause a collision. The deviation is embedded into a $\mathbf{4^{th}}$ order model that estimates the position deviation for a given wind velocity. The maximum position deviation of all the trajectories combined from figure.5.1 is chosen as the safety metric. The Table.4.1 gives a relation between wind velocity and the position deviation.

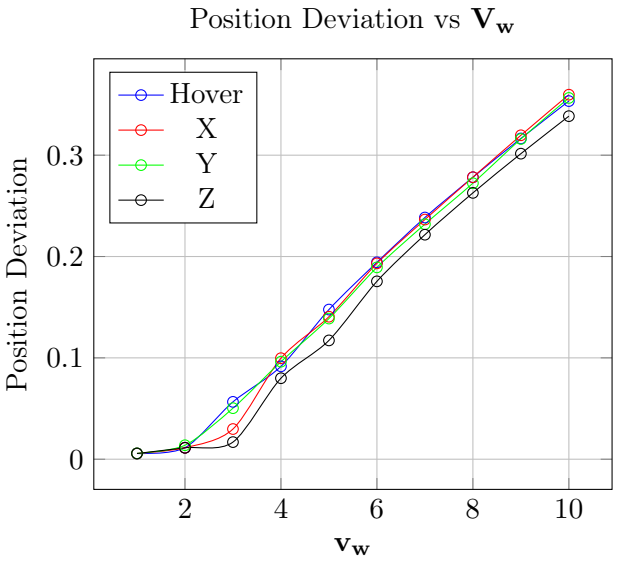

Figure 5.1: Position Deviations for Various Trajectories

To elaborate more on the obstacle avoidance constraint $\|\mathbf{x}(k) - \mathbf{x}_{\text{obs}}(k)\| \geq (r_{\text{rob}} + r_{\text{obs}}) + d_{\text{safe}}$. This is a non-linear constraint that takes into account the norm of the distance between the systems position states ($\mathbf{p}$) and obstacle. The metric provides an estimated additional disturbance due to the given wind. This estimate is a parameter to the system $\mathbf{d_{safe}}$ as a constraint in the controller for each prediction horizon, there by the system maintains a safe distance to the human operator even in the presence of wind. Without the constraint, the controller dynamics is not aware of this additional disturbance and will find it hard to follow the desired state trajectory, highly deviating control inputs and sometimes violate the safety constraint.

6 Simulation and Results

The system defined in the previous sections is simulation under various wind conditions. This chapter encapsulates the complete simulation setup used to evaluate the system and the controller. The system is modeled using **CasADi**'s symbolic framework. The optimal control problem was defined using **acados**, framework. The optimization problem was solved by the controller defined using this framework for given reference state trajectory for various trajectories and the system was further evaluated. The control problem was setup in MATLAB Simulink.

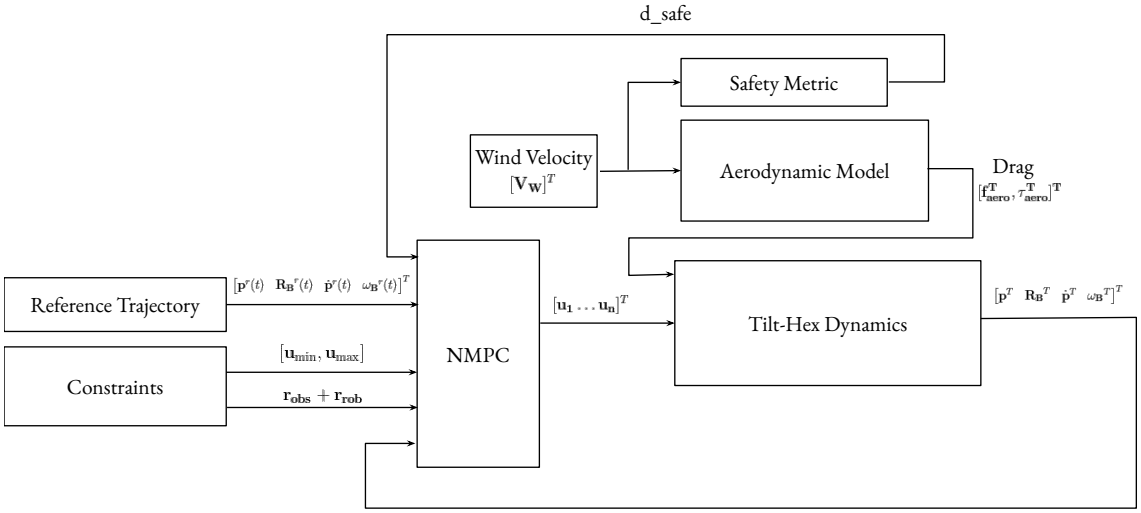

Figure 6.1: Block Diagram of the Simulated System

A brief working of the simulation is provided as a block diagram in the Figure.6.1. Here, The 'Trajectory generation' block provides a set of reference state trajectory that the system is expected to follow. The NMPC is the controller that is tasked to guide the system to reach the desired states of the reference trajectory. There are additional constraints such as limits to the propeller speeds $\mathbf{u_{min}} \dots \mathbf{u_{max}}$ and a geometry based distance $\mathbf{r_{rob}} + \mathbf{r_{obs}}$.

The controller contains the model of the system without the inclusion of the aerodynamic model. This is to evaluate the performance of the system and controller under wind disturbance and also evaluate the performance of the safety metric. The controller provides the control inputs to the dynamic model of the system. These inputs are updated at every time step aimed to ensure the system states converge to desired states.

The 'Tilt-Hex Dynamics' block contains the dynamic model of the hexarotor that produce the actual states of the system for the control input. This block also considers the aerodynamic model that provides the additional drag term due to the wind. Because of this additional disturbance there is expected to be a deviation in the states of the system. The 'Safety Metric' block has a model that predicts the estimated deviation for a particular wind velocity. This estimated deviation is fed into the controller as an additional parameter. This parameter is ($\mathbf{d_{safe}}$) to ensure the system maintains a safe distance to the human in the presence of wind.

The simulation aims to test the working of this system under various reference trajectories under various wind conditions. The performance of the controller and the system is evaluated with and without the safety metric. Table.6.1 are the model parameters that

are used to simulate the hexarotor. These remain constant throughout all the simulations. Table.6.2 detail the simulation and the controller parameters, these parameters influence the performance of the NMPC.

Table 6.1: Model Parameters

Hexarotor Parameters	
UAV mass (m_{uav})	2.25 kg
Inertia along x-axis (I_x)	0.0207 kg·m^2
Inertia along y-axis (I_y)	0.0210 kg·m^2
Inertia along z-axis (I_z)	0.0362 kg·m^2
Propeller length (l_{prop})	0.4 m
Coefficient of Thrust (k_f)	$11.5 \times 10^{-4}\{\mathbf{f}(\varpi, \mathbf{J})\}$
Coefficient of Torque (k_τ)	0.000023884 $\{\mathbf{f}(\varpi, \mathbf{J})\}$
Tilt angle (α)	20 degrees ($\approx$ 0.3491 radians)

Table 6.2: Controller Parameters

Controller Parameters	
Controller Frequency	20 Hz
Simulation Frequency	100 Hz
Prediction Horizon (N)	20 steps
Trajectory Time (T)	5 s
$\mathbf{U_{max}}$	100^2 rpm
$\mathbf{U_{min}}$	16^2 rpm
Integrator Type	
Integrator Type	explicit runge-kutta

6.1 Simulations

6.1.1 Case 0 : Trajectory Tracking with an Obstacle

The NMPC in itself is a robust controller. This means that the solver solves the OCP for various conditions and trajectories quite efficient. To, illustrate, the controller works with an obstacle to track a reference trajectory that is shown in Figure.6.2a under the no wind condition. The overall safe distance that the hexarotor is expected to maintain is $(\mathbf{r}_{\text{rob}} + \mathbf{r}_{\text{obs}}) + \mathbf{d}_{\text{safe}}$. The $\mathbf{d_{safe}}$ here represents the safety distance form the metric previously discussed. In this case there is no wind considered, therefore there is no additional $\mathbf{d_{safe}}$ and the safety distance is the geometry of the system.

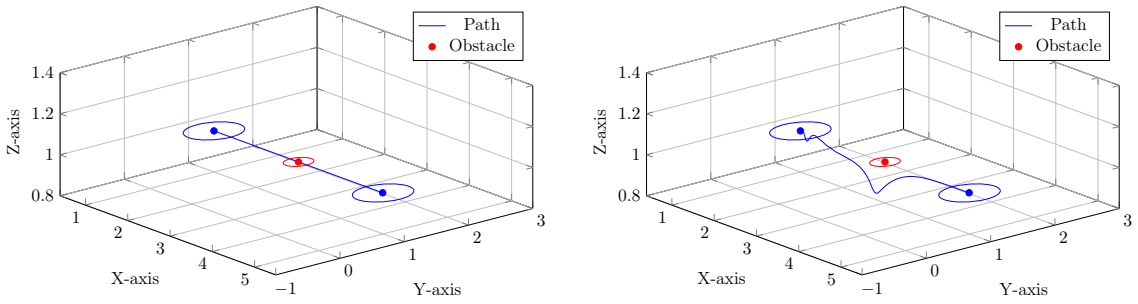

(a) Reference Trajectory **(b)** Simulated Trajectory

Figure 6.2: Case 0 : Trajectory tracking with an Obstacle (Obstacle Avoidance)

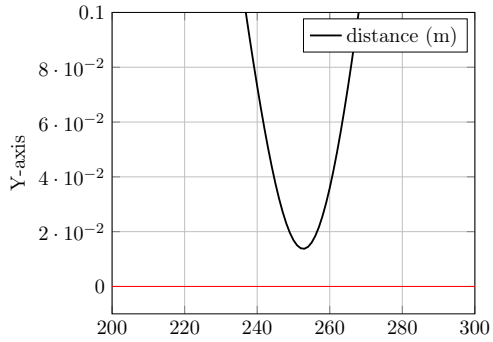

Figure 6.3: Safety Constraint: Distance to violating the safety constraint

The generated trajectory is a trajectory in the X axis from 1m **1m** to **5m**, with the Obstacle at $\{\mathbf{3}, \mathbf{1}, \mathbf{1}\}$. Figure.6.2b depicts the actual trajectory taken by the hexarotor while trying to avoid the obstacle. As it can be seen, the controller is able to solve the OCP, respecting the contraints to maintian a safe distance of **0.1m** to the Obstacle's radius. The trajectory time here is **5sec**, with a 0.01 step.

Figure.6.3 depicts the distance to obstacle. The MPC solves the OCP without any violations to the safety constraint with a margin of **0.0138m**. To MPC is able to solve most trajectories even in the presence of wind with a sufficient enough trajectory time. It is inferred that the NMPC is robust on its own to track trajectories during no wind disturbance.

6.2 Trajectory Tracking with Wind

Figure.6.4 is wind gust that simulates wind in a realistic setup. The wind magnitude increases to a maximum near the obstacle. Two conditions were tested for the following wind velocities $\mathbf{v_w} = \{\mathbf{2.5}, \mathbf{5}, \mathbf{7.5}, \mathbf{10}\}\mathbf{m/s}$, one without the use of safety metric, there are no updates of the expected deviation due to the wind and the other, with the use of safety metric, updates of the expected deviation due to the wind.

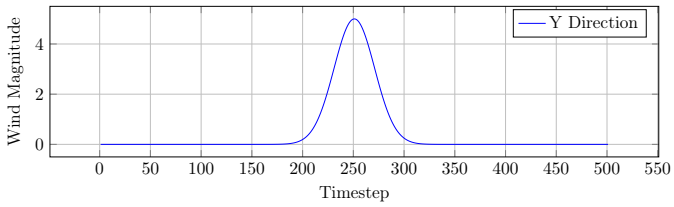

Figure 6.4: Strong Wind Gust for a wind magnitude ($5m/s$)

To test performance of the controller and safety metric. There were several simulations performed with trajectories in various directions and wind gust at different locations. A case that was particularly challenging is presented here.

To elaborate further, there must be sufficient enough wind near the obstacle for it to violate the safety constraint. To test this, instead of considering the obstacle in the reference path. The obstacle is instead at $\{\mathbf{3}, \mathbf{1.2}, \mathbf{1}\}$. In this case, the controller does not have to deviate from its reference path. This tests the performance of the controller because the NMPC does not expect a sudden wind gust. Figure.6.5 illustrates the path that the controller tracks. Considering the wind gust to hit the drone near the obstacle, performance of the controller is evaluated with and without the safety metric. Tracking with the safety metric the controller is able to reach the end without a collision.

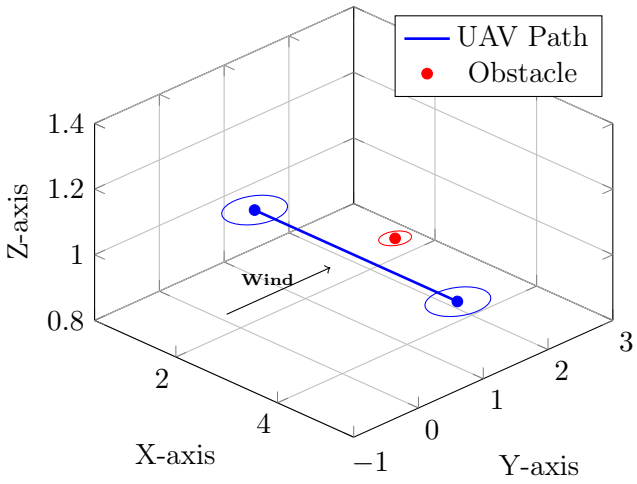

Figure 6.5: Case 1: Simulated Trajectory

6.2.1 Tracking without Safety Metric

To visualize the performace of the controller in the presence of wind, Figure.6.6a shows the distance of the hexarotor to the obstacle. Tracking the reference trajectory can be performed by the controller especially at low wind velocities. But, it is pushed to its limits to ensure that the trajectory is being followed. This produces an undesirable changes in control inputs. At higher wind velocities, the solver does not return a feasible solution. From the trials, the qp_{solver} fails to find a feasible solution due to this wind gust (i.e the UAV does not reach its end position). The distance to violating the safety constraint is very close, in some cases the controller manages to solve, but for wind velocities higher than $\mathbf{5m/s}$ the safety constraint is violated. The distance to violating the safety constraints is detailed further. For $\mathbf{v_w} = \{\mathbf{2.5}, \mathbf{5}, \mathbf{7.5}, \mathbf{10}\}\mathbf{m/s}$ results in $\mathbf{distance}\{\mathbf{0.0088}, -\mathbf{0.0014}, -\mathbf{0.0078}, -\mathbf{0.0085}\}\mathbf{m}$

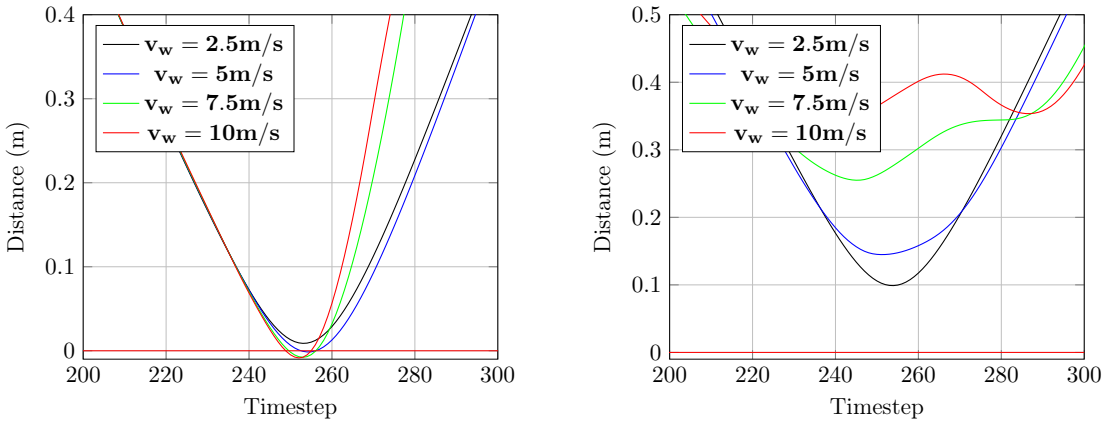

(a) Performance without Safety Metric

(b) Performance with Safety Metric

Figure 6.6: Controller Performance with Wind

6.2.2 Tracking with Safety Metric

The inclusion of the safety metric improves the tracking significantly because the controller is aware of the deviation expected due to the wind. This makes the OCP solve the problem with the updated constraint thereby being more efficient in avoiding the obstacle. Figure.6.6b illustrates this. The distance to violating the safety constraints for $\mathbf{v_w} = \{\mathbf{2.5}, \mathbf{5}, \mathbf{7.5}, \mathbf{10}\}\mathbf{m/s}$ are $\{\mathbf{0.0989}, \mathbf{0.1448}, \mathbf{0.2549}, \mathbf{0.3475}\}\mathbf{m}$.

6.2.3 Using the Safety Metric

In a real world scenario, the maximum wind speed for a particular day is measured (detailed here) and that is considered as the $\mathbf{v_w}$. The safety metric then provides the expected deviation due to this wind and this is added as an additional distance constraint that the system has to respect. With this, the planner will plan a trajectory that avoids collision. Therefore ensuring safe human-aerial robot collaboration.

7 Discussion and Conclusion

7.1 Trajectories in Different Directions

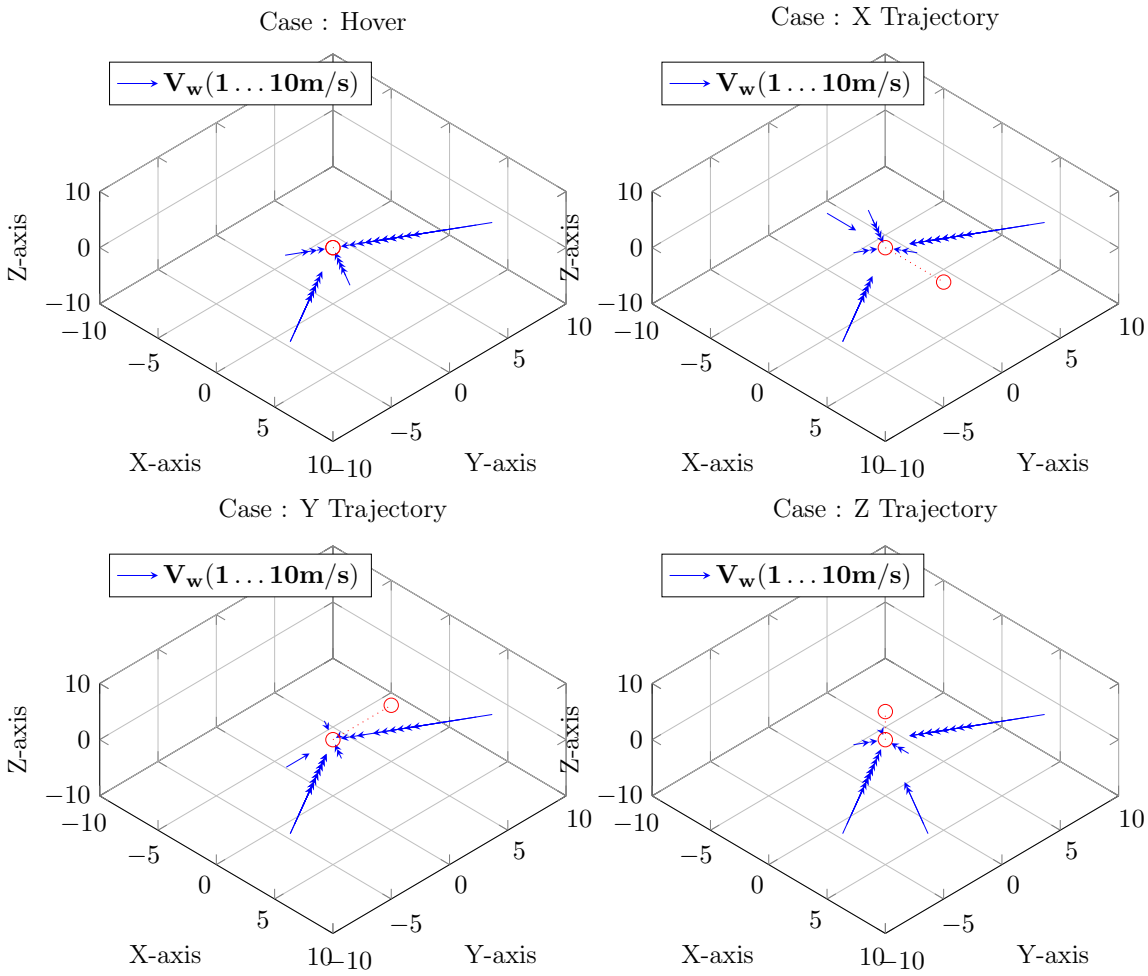

Figure 7.1: Wind Directions for maximum position displacement: The hexarotor moves 5m in the direction of the cases Hover, X, Y and Z. The figure also contains the 6 wind vectors that produce the biggest deviation in position for all 62 cases mentioned here 4.1. Red dots represent the trajectory of the hexarotor.

Figure.7.1 illustrates all the wind directions that produce a maximum deviation in the position of the hexarotor. The hexarotor is tasked to take trajectories in X, Y ,Z directions with the wind disturbw for wind out of the 62 different directions (previously detailed in Section4.1) is illustrated in Figure.7.1. It can be inferred that overall, regardless of the wind direction the position deviation is a maximum for a wind direction in the horizontal X-Y plane. The safety metric incorporates this deviation as the safety distance. Table.4.1 detailed in the safety metric chapter. Concludes that the deviation in position error for all the 4 trajectory cases (hover, X, Y, Z) is minimum.

Since, the hexarotor is fully actuated, this can be extended to more complicated trajectories. Based on the wind, the safety metric will provide the controller additional constraint to satisfy. This will extend to a more safer distance to the human operator, minimizing risk of collision.

7.2 Conclusion

In this thesis, a safety metric was constructed that guides the robot's motion in the presence of aerodynamic disturbances. It enables safe human-aerial robot collaboration task in the presence of wind disturbance.

A tilted-axis hexarotor system is utilized with information from the aerodynamic model. The system is simulated in various wind conditions to test the performance of the safety metric. To construct this safety metric, the tilted-axis hexarotor system and integrated information from an aerodynamic model is used to assess the impact of wind disturbances. This is simulated under various wind conditions to obtain the metric. A look-up table that represents the deviation in robot's position is obtained. Deviation due to several wind directions are analyzed in the simulation. The metric is incorporated in an NMPC framework to optimize the system in the presence of wind. The controller is efficient in handling non-linear dynamics and constraints. The metric is embedded in the constraints enabling safe operation in a collaboration task with a human operator.

The performance of the safety metric is evaluated through simulations involving various wind conditions and trajectories. These simulations demonstrated that the safety metric helps the system's ability to maintain safe operation in the presence of wind disturbances. The aerodynamic effects of wind are incorporated in the safety. Simulations shows that the controller with safety metric guides the hexarotor system to complete a trajectory task for safe human-aerial robot collaboration in presence of dynamic wind environments.

7.3 Recommendations

The safety metric cane be made more robust by considering complex wind models to build the look-up table. The tilt-hex dynamic model can be used as reference to deploy other robot models into similar simulations to obtain a safety metric for the other systems.

One approach would be to tune the controller even more for various wind directions and optimize the control inputs. This involves testing the system in more complex simulations with dynamic obstacles. This can be extended to more complex wind models.

The other natural progression is to simulate this system in a more realistic physics simulator like Gazebo. The "Genom" framework with "robotpkg" can be utilized to connect everything together. Connecting MATLAB/Simulink with Gazebo and ROS (Robot Operating Systems) offers more opportunities to test against other robust controllers.

A Appendix

A.1 Allocation Matrix for the TiltHex

In section. 3.1 equations 3.15 and 3.16 represent the dynamic model of tilt-hex. The terms $\mathbf{F}(\alpha, \beta, \gamma)\mathbf{u}$ and $\mathbf{H}(\alpha, \beta, \gamma, \mathbf{L})\mathbf{u}$ are expanded here, to be precise 3.2 and 3.7. Expanding the rotational matrices we get,

$$\begin{bmatrix} F \\ H \end{bmatrix} = \begin{bmatrix} 0 & -\frac{\sqrt{3}}{2}k_f s_\alpha & \frac{\sqrt{3}}{2}k_f s_\alpha & 0 & -\frac{\sqrt{3}}{2}k_f s_\alpha & \frac{\sqrt{3}}{2}k_f s_\alpha \\ -k_f s_\alpha & \frac{1}{2}k_f s_\alpha & \frac{1}{2}k_f s_\alpha & -k_f s_\alpha & \frac{1}{2}k_f s_\alpha & \frac{1}{2}k_f s_\alpha \\ k_f c_\alpha & k_f c_\alpha & k_f c_\alpha & k_f c_\alpha & k_f c_\alpha & k_f c_\alpha \\ 0 & \frac{\sqrt{3}}{2}k_\tau s_\alpha + \frac{\sqrt{3}}{2}Lk_f c_\alpha & \frac{\sqrt{3}}{2}k_\tau s_\alpha + \frac{\sqrt{3}}{2}Lk_f c_\alpha & 0 & -\frac{\sqrt{3}}{2}k_\tau s_\alpha + \frac{\sqrt{3}}{2}Lk_f c_\alpha & -\frac{\sqrt{3}}{2}k_\tau s_\alpha + \frac{\sqrt{3}}{2}Lk_f c_\alpha \\ -k_\tau s_\alpha - Lk_f c_\alpha & -\frac{1}{2}k_\tau s_\alpha - \frac{1}{2}Lk_f c_\alpha & \frac{1}{2}k_\tau s_\alpha - \frac{1}{2}Lk_f c_\alpha & k_\tau s_\alpha - Lk_f c_\alpha & \frac{1}{2}k_\tau s_\alpha - \frac{1}{2}Lk_f c_\alpha & -\frac{1}{2}k_\tau s_\alpha - \frac{1}{2}Lk_f c_\alpha \\ k_\tau c_\alpha - Lk_f s_\alpha & Lk_f s_\alpha - k_\tau c_\alpha & k_\tau c_\alpha - Lk_f s_\alpha & Lk_f s_\alpha - k_\tau c_\alpha & k_\tau c_\alpha - Lk_f s_\alpha & Lk_f s_\alpha - k_\tau c_\alpha \end{bmatrix} \tag{A.1}$$

Here, k_f & k_τ are the force and torque coefficients, s_α & c_α are the *sin* and *cosine* of the tilt angle (α). L is the distance from propeller to the center of body frame.

Bibliography

[1] Florian Achermann, Nicholas R. J. Lawrance, René Ranftl, Alexey Dosovitskiy, Jen Jen Chung, and Roland Siegwart. Learning to predict the wind for safe aerial vehicle planning. In *2019 International Conference on Robotics and Automation (ICRA)*, pages 2311–2317, 2019.

[2] Amr Afifi, Mark van Holland, and Antonio Franchi. Toward physical human-robot interaction control with aerial manipulators: Compliance, redundancy resolution, and input limits. In *2022 International Conference on Robotics and Automation (ICRA)*, pages 4855–4861. IEEE, 2022.

[3] Bárbara Barros Carlos, Antonio Franchi, and Giuseppe Oriolo. Towards safe human-quadrotor interaction: Mixed-initiative control via real-time nmpc. *IEEE Robotics and Automation Letters*, 6(4):7611–7618, 2021.

[4] John Brandt and Michael Selig. Propeller performance data at low reynolds numbers. In *49th AIAA Aerospace Sciences Meeting including the New Horizons Forum and Aerospace Exposition*, page 1255, 2011.

[5] Elisabetta Cataldi, Giuseppe Muscio, Miguel Angel Trujillo, Yamnia Rodríguez, Francesco Pierri, Gianluca Antonelli, Fabrizio Caccavale, Antidio Viguria, Stefano Chiaverini, and Aníbal Ollero. Impedance control of an aerial-manipulator: Preliminary results. In *2016 IEEE/RSJ International Conference on Intelligent Robots and Systems (IROS)*, pages 3848–3853. IEEE, 2016.

[6] Gianluca Corsini, Martin Jacquet, Hemjyoti Das, Amr Afifi, Daniel Sidobre, and Antonio Franchi. Nonlinear model predictive control for human-robot handover with application to the aerial case. In *2022 IEEE/RSJ International Conference on Intelligent Robots and Systems (IROS)*, pages 7597–7604. IEEE, 2022.

[7] Brittany A Duncan and Robin R Murphy. Autonomous capabilities for small unmanned aerial systems conducting radiological response: Findings from a high-fidelity discovery experiment. *Journal of Field Robotics*, 31(4):522–536, 2014.

[8] Ohad Gur and Aviv Rosen. Propeller performance at low advance ratio. *Journal of aircraft*, 42(2):435–441, 2005.

[9] Jérémy Jessin, Charlotte Heinzlef, Nathalie Long, and Damien Serre. A systematic review of uavs for island coastal environment and risk monitoring: Towards a resilience assessment. *Drones*, 7(3):206, 2023.

[10] Guangying Jiang, Richard M. Voyles, and Jae Jung Choi. Precision fully-actuated uav for visual and physical inspection of structures for nuclear decommissioning and search and rescue. In *2018 IEEE International Symposium on Safety, Security, and Rescue Robotics (SSRR)*, pages 1–7, 2018.

[11] Taeyoung Lee, Melvin Leok, and N Harris McClamroch. Geometric tracking control of a quadrotor uav on se (3). In *49th IEEE conference on decision and control (CDC)*, pages 5420–5425. IEEE, 2010.

[12] Changan Liu, Yang Liu, Hua Wu, and Ruifang Dong. A safe flight approach of the uav in the electrical line inspection. *International Journal of Emerging Electric Power Systems*, 16(5):503–515, 2015.

[13] Monal Merchant and L Scott Miller. Propeller performance measurement for low reynolds number uav applications. In *44th AIAA aerospace sciences meeting and exhibit*, page 1127, 2006.

[14] Sarah L Murfitt, Blake M Allan, Alecia Bellgrove, Alex Rattray, Mary A Young, and Daniel Ierodiaconou. Applications of unmanned aerial vehicles in intertidal reef monitoring. *Scientific reports*, 7(1):10259, 2017.

[15] Anibal Ollero, Guillermo Heredia, Antonio Franchi, Gianluca Antonelli, Konstantin Kondak, Alberto Sanfeliu, Antidio Viguria, J Ramiro Martinez-de Dios, Francesco Pierri, Juan Cortés, et al. The aeroarms project: Aerial robots with advanced manipulation capabilities for inspection and maintenance. *IEEE Robotics & Automation Magazine*, 25(4):12–23, 2018.

[16] Anibal Ollero, Marco Tognon, Alejandro Suarez, Dongjun Lee, and Antonio Franchi. Past, present, and future of aerial robotic manipulators. *IEEE Transactions on Robotics*, 38(1):626–645, 2021.

[17] Sammy Omari, Minh-Duc Hua, Guillaume Ducard, and Tarek Hamel. Hardware and software architecture for nonlinear control of multirotor helicopters. *IEEE/ASME Transactions on mechatronics*, 18(6):1724–1736, 2013.

[18] Sujit Rajappa, Markus Ryll, Heinrich H Bülthoff, and Antonio Franchi. Modeling, control and design optimization for a fully-actuated hexarotor aerial vehicle with tilted propellers. In *2015 IEEE international conference on robotics and automation (ICRA)*, pages 4006–4013. IEEE, 2015.

[19] Mukhtar Sani, Bogdan Robu, and Ahmad Hably. Dynamic obstacles avoidance using nonlinear model predictive control. In *IECON 2021–47th annual conference of the IEEE industrial electronics society*, pages 1–6. IEEE, 2021.

[20] MAR Silvestre, J Morgado, P Alves, P Santos, P Gamboa, and JC Páscoa. Propeller performance measurements at low reynolds numbers. *International Journal of Mechanics*, 9:154–166, 2015.

[21] Marco Tognon, Hermes A Tello Chávez, Enrico Gasparin, Quentin Sablé, Davide Bicego, Anthony Mallet, Marc Lany, Gilles Santi, Bernard Revaz, Juan Cortés, et al. A truly-redundant aerial manipulator system with application to push-and-slide inspection in industrial plants. *IEEE Robotics and Automation Letters*, 4(2):1846–1851, 2019.

[22] Teodor Tomić and Sami Haddadin. A unified framework for external wrench estimation, interaction control and collision reflexes for flying robots. In *2014 IEEE/RSJ international conference on intelligent robots and systems*, pages 4197–4204. IEEE, 2014.

[23] Teodor Tomić, Philipp Lutz, Korbinian Schmid, Andrew Mathers, and Sami Haddadin. Simultaneous contact and aerodynamic force estimation (s-cafe) for aerial robots. *The International Journal of Robotics Research*, 39(6):688–728.

[24] Teodor Tomić and Sami Haddadin. Simultaneous estimation of aerodynamic and contact forces in flying robots: Applications to metric wind estimation and collision detection. In *2015 IEEE International Conference on Robotics and Automation (ICRA)*, pages 5290–5296, 2015.